Numerical study for the design and optimization of direct absorption solar collectors with carbon-based nanofluids

Gabellone, Mario Junio; Berto, Arianna; Zanetti, Emanuele; Del Col, Davide

Important note
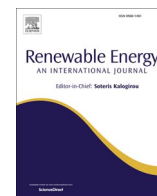To cite this publication, please use the final published version (if applicable).
Please check the document version above.

Numerical study for the design and optimization of direct absorption solar collectors with carbon-based nanofluids

Mario Junio Gabellone [a], Arianna Berto [a,*], Emanuele Zanetti [b] , Davide Del Col [a]

[a] *University of Padova, Department of Industrial Engineering, Via Venezia 1, 35131, Padova, Italy*
[b] *Department of Process and Energy, Delft University of Technology, Leeghwaterstraat 39, 2628 CB, Delft, the Netherlands*

ABSTRACT

Solar thermal collectors are crucial for decarbonizing thermal energy needs in both residential and industrial sectors. However, improving thermal efficiency remains a key challenge for this technology, as it is significantly affected by the conductive and convective thermal resistances between the working fluid and the absorber. Additionally, reducing investment costs is necessary for widespread adoption. To overcome these issues, Direct Absorption Solar Collectors (DASCs) using nanofluids with tailored optical properties have been proposed. In DASCs, the working fluid directly absorbs the solar radiation and converts it into heat, which simplifies the system's design and improves the temperature distribution within the fluid, therefore enhancing the overall thermal efficiency.

The present study involves numerical simulations in ANSYS Fluent to evaluate the thermal performance of two DASCs: a flat rectangular and an evacuated tube configuration. Both systems operate with carbon nanofluids, specifically Single-Wall-Carbon-NanoHorns (SWCNHs) suspended in deionized water. The impact of nanofluid temperature and mass flow rate, nanoparticles' concentration, glass properties and geometrical features on thermal efficiency is thoroughly analyzed.

The optimization of DASC geometry, proper material selection and tuning of nanoparticles' concentration are found to be crucial for the future deployment of DASCs in the building sector, ensuring higher performance and cost-effectiveness.

1. Introduction

According to the latest outlook of the International Energy Agency (IEA), a 40 % global increase in the heat demand is expected during the period 2023–2028 [1]. Solar thermal collectors at low and medium temperature (below 200 °C) have proved to be a reliable solution to supply heat and decarbonize the residential and industrial sectors, in compliance with European and worldwide regulations [2,3].

The possible market for solar thermal collectors is becoming wider, especially considering the gradual ban on sales of new fossil fuel-fired boilers. In 2023 the global solar thermal energy yield from all installed systems led to savings of 49.1 million tons of oil and 158.4 million tons of CO_2. This underscores the substantial contribution of this technology towards mitigating global greenhouse gas emissions [4].

To fully harness the capabilities of solar thermal solutions, it is crucial to foster technological advancement, especially considering the increasing share of renewables that will need to be integrated into energy systems in the future [5,6]. In particular, the annual rate of solar thermal energy exploitation should double to align with the IEA Net Zero scenario, which foresees zero emissions by mid-century, implying much more efforts to improve the efficiency of existing solar heating systems [1].

Conventional solar thermal collectors rely on indirect absorption, where a blackened absorber plate converts sunlight into heat, which is then transferred to a working fluid through conductive and convective thermal resistances. However, such systems are affected by major thermal losses due to the high temperatures reached at the absorber surface. A promising alternative is offered by direct absorption solar collectors (DASCs) where the sunlight is absorbed directly within the volume of the heat transfer fluid itself, whose optical properties must be optimized. This solution could lead to a technological simplification (due to the absence of the selective absorber) and, under certain

---

This article is part of a special issue entitled: SDEWES2024 published in Renewable Energy.

* Corresponding author

E-mail address: arianna.berto@unipd.it (A. Berto).

configurations, to a better temperature distribution within the solar receiver [7,8].

In recent years, suspensions of nanometric particles in water or other liquids, also known as nanofluids, have attracted significant attention for their employment in DASCs [9]. In particular, carbon-based nanofluids display excellent chemical stability and broad absorption spectrum characteristics. Optical properties have been extensively investigated in the literature, showing that small concentrations of nanoparticles (less than 1 g/L) result in a significant enhancement of the absorption capability of the fluid [10,11]. Several research studies have shown experimentally [12,13], analytically and numerically [14,15] that nanofluids can sensibly enhance the thermal performance of DASCs.

While most studies in the field focus on high-temperature and high-flux nanofluid solar collectors [16,17], low-temperature DASCs with applicability for domestic solar heating systems have not been sufficiently investigated. Some experimental works have reported efficiency gains of up to 30 % in tubular DASCs using water-based carbon nanofluids, with thermal efficiency increasing asymptotically with both volume fraction and flow rate [18–20].

Recent CFD-based studies have also investigated the influence of various parameters on the thermal performance of DASCs, particularly nanoparticles' concentration, flow conditions, base fluid properties and collector geometry [21,22]. Direct absorption systems have demonstrated superior performance under high thermal loss conditions, such as high-transmittance glazing or elevated fluid temperatures, and with increasing nanoparticles' concentrations, up to an optimal threshold beyond which thermal efficiency tends to decline [23].

These findings underscore the crucial importance of accurate design, careful material selection, and appropriate configuration choices to maximize the thermal performance of DASC systems.

In a previous experimental study performed by the present authors [24], the thermal efficiency of a flat volumetric solar collector working with Single-Wall-Carbon-NanoHorns (SWCNHs) suspensions was found to be between 88 % and 92 % at ambient temperature. However, with the increasing temperature difference between the nanofluid and the external environment, the thermal efficiency steeply decreased due to the higher convective/radiative thermal losses through the glazed surface and the non-optimized geometry of the receiver.

To overcome this drawback, the present study aims at developing new design strategies for volumetric solar collectors operating with carbon nanofluids, considering a vacuum tube type (or evacuated) DASC which is expected to display smaller thermal losses compared to the flat one, especially at high working temperatures. This configuration is particularly relevant for building-integrated solar thermal systems operating at low temperatures but requiring year-round performance.

The considered nanofluid is made of Single-Wall Carbon NanoHorns (SWCNHs), which offer several key advantages over traditional carbon nanotubes (CNTs). In contrast to CNTs, SWCNHs are produced without metal catalysts, thereby eliminating residual catalyst impurities that have been linked to CNT cytotoxicity [25]. This inherently low cytotoxicity makes SWCNHs well-suited for nanofluid formulations and for applications where accidental environmental release may occur, as the potential impact on living organisms is significantly reduced. Moreover, the unique conical ("horn") morphology of SWCNHs reduces interparticle van der Waals attractions, resulting in markedly improved dispersion stability without the need for prolonged sonication or high surfactant loads [26,27].

A detailed numerical model is developed in ANSYS Fluent, enabling a comparative analysis between flat and evacuated tube DASC configurations. The model evaluates the optical and thermal performance of each configuration and investigates the influence of several design and operating parameters: nanofluid temperature, mass flow rate, nanoparticles' concentration, collector geometry (including triple-tube structures) and the glass properties.

The novelty of the present work lies in the following aspects:

- Proposing an evacuated tube DASC tailored for low-temperature civil applications;
- Employing carbon nanohorn-based nanofluids, that despite their promising optical absorption characteristics and high surface area are less commonly used than carbon nanotubes due to their higher production costs and limited commercial availability. This work contributes to expanding their applicability by assessing their performance in realistic collector configurations;
- Performing a comparative numerical analysis of two collector geometries, flat plate and evacuated tube, unlike most existing studies, which typically focus on a single configuration. This dual-geometry approach allows for a clearer assessment of the respective advantages and limitations of each system, providing valuable design guidelines for different use cases;
- Highlighting the advantages of volumetric absorption in combination with vacuum insulation, with direct implications for the next generation of high-efficiency solar thermal systems.

This research contributes to filling the existing technology gap in the field of solar thermal energy, by offering design guidelines and performance insights for efficient and compact DASCs suitable for residential and industrial energy systems.

2. Methodology

This section outlines the methodology adopted to analyze the thermal and optical performance of a flat and an evacuated tube DASC. A 3D numerical model is developed in ANSYS Fluent to simulate the heat and fluid flow dynamics in both systems. The following sub-sections detail the model architecture and the validation procedure based on experimental data.

2.1. Description of the numerical model

Numerical simulations of different configurations of DASCs are performed in ANSYS Fluent 22.2 to evaluate their thermal performance with varying operating conditions. For all the simulations involving flows with temperature changes, ANSYS Fluent solves the mass, momentum and energy conservation equations over time (t):

$$\frac{\partial \rho}{\partial t} + \nabla \cdot (\rho \, \overrightarrow{v}) = 0 \tag{1}$$

$$\frac{\partial}{\partial t} (\rho \, \overrightarrow{v}) + \nabla \cdot (\rho \, \overrightarrow{v} \, \overrightarrow{v}) = -\nabla p + \nabla \overline{\overline{\tau}}_s + \rho \, \overrightarrow{g} \tag{2}$$

$$\frac{\partial}{\partial t} (\rho \, E) + \nabla \cdot [\overrightarrow{v} \, (\rho \, E + p)] = \nabla \cdot (k_{eff} \nabla T) + S_h \tag{3}$$

where p is the pressure, $\overline{\overline{\tau}}_s$ is the stress tensor, $\rho \, \overrightarrow{g}$ is the acceleration due to gravity, k_{eff} is the effective thermal conductivity, E is the total specific energy, $\overrightarrow{v}$ is the velocity vector, ρ is the density, T is the temperature and S_h is a source term related to heat generation which in the present study is represented by the radiation reaching the fluid bulk.

The solar radiation incident on the DASC is modelled with the Monte Carlo method, which is based on stochastic ray tracing. For opaque bodies, this process involves computing the difference between the sum of all energies absorbed by each *j*-th surface and all energies emitted by the same surface. The net balance is given by the following equation:

$$q_j = \left[\sum \left(q_{inc} - q_{refl} \right) - \sum q_e \right]_j \tag{4}$$

where q_j is the resulting energy on the *j*-th surface, q_{inc} is the energy incident on a surface, q_{refl} is the energy reflected from a surface and q_e is the energy emitted by the surface.

This process must be carried out for each direction, position and

wavelength considered. For semi-transparent bodies, scattering and absorption of radiation between surfaces must be considered. In this case, the radiation transfer equation needs to be numerically integrated by discretizing the path of rays crossing a semi-transparent medium into intervals defined by the mesh size.

The radiation transfer equation (RTE) mathematically describes the irradiance propagation through a medium. For a medium that can absorb, emit and scatter radiation at a position $\overrightarrow{r}$ in the direction $\overrightarrow{s}$, the RTE equation can be defined as follows:

$$\frac{dI(\overrightarrow{r}, \overrightarrow{s})}{ds} = -(a_s + \sigma_s) I (\overrightarrow{r}, \overrightarrow{s}) + a n^2 \frac{\sigma_b T^4}{\pi}$$
$$+ \frac{\sigma_s}{4 \pi} \int_0^{4\pi} I (\overrightarrow{r}, \overrightarrow{s}') \Phi (\overrightarrow{s} \cdot \overrightarrow{s}') \, d\Omega' \tag{5}$$

where I is the intensity of incident radiation, $\overrightarrow{r}$ is the position vector, $\overrightarrow{s}$ is the direction vector, $\overrightarrow{s}'$ is the scattering direction vector, s is the distance travelled by radiation through the medium, a_s is the absorption coefficient, n is the refractive index, σ_s is the scattering coefficient, σ_b is the Stefan-Boltzmann constant, T is the local temperature, Φ is the scattering phase function and Ω' is the solid angle.

The $k\text{-}\omega$ SST method [28] is applied to model the turbulence in the nanofluid flow. The thermo-physical properties of the nanofluid are assumed to be analogous to the base fluid (water in this case), due to the small concentration of carbon nanoparticles considered in this work. This was checked in a previous experimental study by the same authors [12].

In the present paper, two DASCs with different configurations are simulated: the first consists of a flat rectangular receiver with two parallel glass layers (Fig. 1a), which was experimentally tested [29,30], and the second is an evacuated tube solar receiver (Fig. 1b). The flat DASC consists of two glasses with dimensions of 500 × 64 mm and thickness of 3 mm each, creating an 18 mm wide passage for the nanofluid flow. Low-iron transparent glass sheets with anti-reflective coating are considered to increase transmittance and reduce reflection losses. The inlet, outlet and side walls of both the nanofluid and the receiver are considered adiabatic since the flat DASC is insulated with a layer of Armaflex® and a reflective aluminium tape to avoid thermal losses.

The evacuated tube receiver consists of three glass tubes with outer diameters of 47 mm, 37 mm and 21.8 mm respectively, each with a thickness of 1.6 mm and length of 1.8 m. Between the two external tubes an annulus under vacuum is placed, to reduce heat losses by convection. The nanofluid flows in an annular section between the internal and the intermediate glass tubes. The inner glass wall is considered adiabatic as it exchanges heat with the air present in the central part of the DASC.
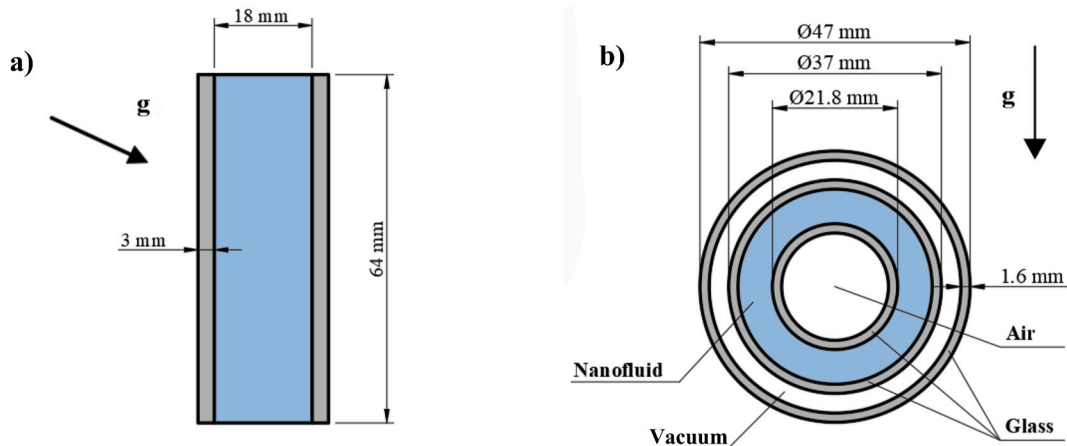
The glass thermal and transport properties are obtained directly from the manufacturer's datasheets. For the SWCNH-based nanofluid, the same thermodynamic and transport properties of water are assumed, since previous studies demonstrated that only its optical behaviour varies with nanoparticles' concentration [12].

The absorption coefficients of both glass and nanofluid are obtained as function of the wavelength by dividing the experimental absorption spectrum into six spectral bands (300–630 nm, 630–1100 nm, 1100–1300 nm, 1300–2100 nm, 2100–2400 nm and above 2400 nm) using a MATLAB script and calculating the mean value in each band. In the case of the nanofluid, the Lambert-Beer law is applied to derive the extinction coefficient in each band, starting from the nanofluid concentration and optical path length.

Conservatively, scattering is set to 5 % of the extinction coefficient in each band, as experimentally confirmed by Mercatelli et al. [31]. Since ANSYS Fluent cannot accept different scattering coefficients per spectral band, a single and constant scattering coefficient, equal to the average of the six band-specific values, is assumed in all simulations.

The average optical properties for each spectral interval are reported in Table 1 for both the nanofluid and the glasses.

The outer glasses of the receivers are involved in convective and radiative heat exchanges, which are respectively computed as follows:

$$q_{conv} = h_{ext} (T_{amb} - T_{wall}) \tag{6}$$

Table 1
Optical properties of the nanofluid and the glass (λ wavelength, n refractive index, a absorption coefficient, σ_s scattering coefficient).

	λ [nm]	n [–]	a [m^{-1}]	σ_s [m^{-1}]
Nanofluid	300–630	1.340	993	42.44
	630–1100	1.328	445	
	1100–1300	1.323	365	
	1300–2100	1.314	2386	
	2100–2400	1.29	1662	
	Above 2400	1.27	3244	
Antireflective Glass	300–630	1.198	2.71	0
	630–1100	1.275	4.89	
	1100–1300	1.292	5.41	
	1300–2100	1.282	5.09	
	2100–2400	1.408	9.65	
	Above 2400	1.045	1479	
Floated Glass	300–630	1.48	1.7	0
	630–1100	1.475	9	
	1100–1300	1. 475	9	
	1300–2100	1. 475	9	
	2100–2400	1.46	27.9	
	Above 2400	1.46	5000	

Fig. 1. Cross-sectional view of the flat volumetric solar receiver (a) and the evacuated tube volumetric solar collector (b). The direction of gravity acceleration is also indicated.

$$q_{rad} = \varepsilon\, \sigma_b \left(T_{sky}^4 - T_{wall}^4 \right) \tag{7}$$

where h_{ext} is the convective heat transfer coefficient with the environment, T_{amb} is the ambient temperature, T_{wall} is the temperature of the surface involved in the heat exchange, ε is the emissivity of the glass, and T_{sky} is the equivalent sky temperature.

The equivalent sky temperature T_{sky} is calculated using the following equations [23]:

$$T_{sky} = 0.0552\, T_{amb}^{1.5} \quad (\text{if } G \leq 100 \text{ W m}^{-2}) \tag{8}$$

$$T_{sky} = T_{amb} \left[0.7 + 0.006\, T_{dew} + 0.00007\, T_{dew} + 0.013\, cos(t) \right]^{1/4} \quad \left(\text{if } \frac{G_{DIF}}{G} \leq 0.7 \right) \tag{9}$$

$$T_{sky} = 94 + 12.6\, ln\left[p_{sat}(T_{amb}) \right] - 13 \left(\frac{G_H}{1360} \right) + 0.341\, T_{amb} \quad \left(\text{if } \frac{G_{DIF}}{G} > 0.7 \right) \tag{10}$$

where T_{dew} is the dew point temperature of the air, t is the time expressed in hours, G_{DIF} is the diffuse irradiance, G is the global irradiance on the collector plane, p_{sat} is the saturation pressure at ambient temperature and G_H is the global irradiance on the horizontal plane. Eqs. 9 and 10 distinguish between the case of clear sky ($G_{DIF}/G \leq 0.7$) and the case of cloudy sky ($G_{DIF}/G > 0.7$).

The portion of the receiver exposed to the sky exchanges heat through convection with the external air temperature and through radiation with the sky. Meanwhile, the part of the receiver facing the ground exchanges heat with the external environment via convection (Eq. 6) and with the ground itself through radiation. Eq. (7) is used for the latter, where the ground temperature (assumed to be equal to the ambient one) is used instead of T_{sky}.

Regarding the external convection heat transfer coefficient h_{ext}, a conservative value of 17 W m^{-2} K^{-1} is chosen by applying the relationship proposed by McAdams [32] where the average wind speed during the experiments (around 2–3 m s^{-1}) is used:

$$h_{ext} = 5.7 + 3.8\, v_{air} \tag{11}$$

where v_{air} is the air speed.

The direction of the solar rays is assumed to be perpendicular to the collector plane in the case of the flat receiver and to the projected area of the DASC on a horizontal plane in the case of the vacuum-type collector. In the case of the flat collector, the direction of the gravitational acceleration is inclined by approximately 23°, in order to reproduce the inclination of the solar receiver during the experiments, which was kept almost perpendicular to the solar rays.

Additional simulations were carried out to assess the potential influence of collector inclination (i.e., variations in the gravitational acceleration components) on the thermal behaviour of both flat and evacuated volumetric collectors. The effect was found to be negligible under the considered configurations and operating conditions, particularly in terms of temperature distributions inside the collectors; therefore, inclination-related aspects are not discussed in the present work.

Parabolic reflectors, potentially coupled with the evacuated tube

volumetric solar collector, are not modelled in the present study.

Table 2 summarizes the boundary conditions set for the numerical simulations.

A sensitivity analysis is conducted to define the mesh size and the number of subdivisions for each of the spatial dimensions of the DASC. The mesh refinement is performed until the percent deviation in terms of thermal efficiency is less than 3 %.

The computational grid is generated with particular attention to the near-wall resolution. In all simulations, the first grid node off the wall is placed so that the non-dimensional wall distance y^+ remains below unity over the entire solid surface. This mesh refinement guarantees full resolution of the viscous sub-layer and fulfils the near-wall requirements of the k-ω SST turbulence model.

The adopted grid for both the flat DASC and the evacuated tube solar receiver, resulting from the sensitivity analysis, is shown in Fig. 2. The number of elements is in the order of 10^5 for both geometries.

2.2. Validation of the numerical model

The numerical model has been validated using the experimental data obtained on a flat volumetric solar receiver displaying the same dimensions as the simulated one.

The experimental setup considered for testing is shown in Fig. 3a) and consists of a nanofluid loop and an auxiliary water circuit. The nanofluid is heated up or cooled down in a tube-in-tube heat exchanger using water, which flows in counter-current in the external annulus. The nanofluid is then sent to the volumetric solar receiver under test by an inverter-controlled rotary vane pump. The nanofluid mass flow rate is evaluated using a Coriolis mass flow meter (accuracy: $\pm$ 0.1 % of the reading at $\dot{m}_n \geq 14$ kg h^{-1}, $\pm$ 0.27 % of the reading at $\dot{m}_n = 5$ kg h^{-1}).

The tested volumetric solar receiver consists of two rectangular anti-reflective glass sheets (size 500 × 60 × 3 mm), embedded in two stainless steel frames, and three PEEK layers combined to form the 18 mm deep channel for the nanofluid passage. The test rig is mounted on a movable cart which allows to vary the azimuth and tilt angle of the system in order to follow the sun position and keep the receiver almost perpendicular to the solar radiation (incidence angle lower than 2.5°).

PT-100 type RTDs (accuracy: ±0.03 K) are used to measure the

Table 2
Boundary conditions for the numerical simulations of the volumetric solar receivers.

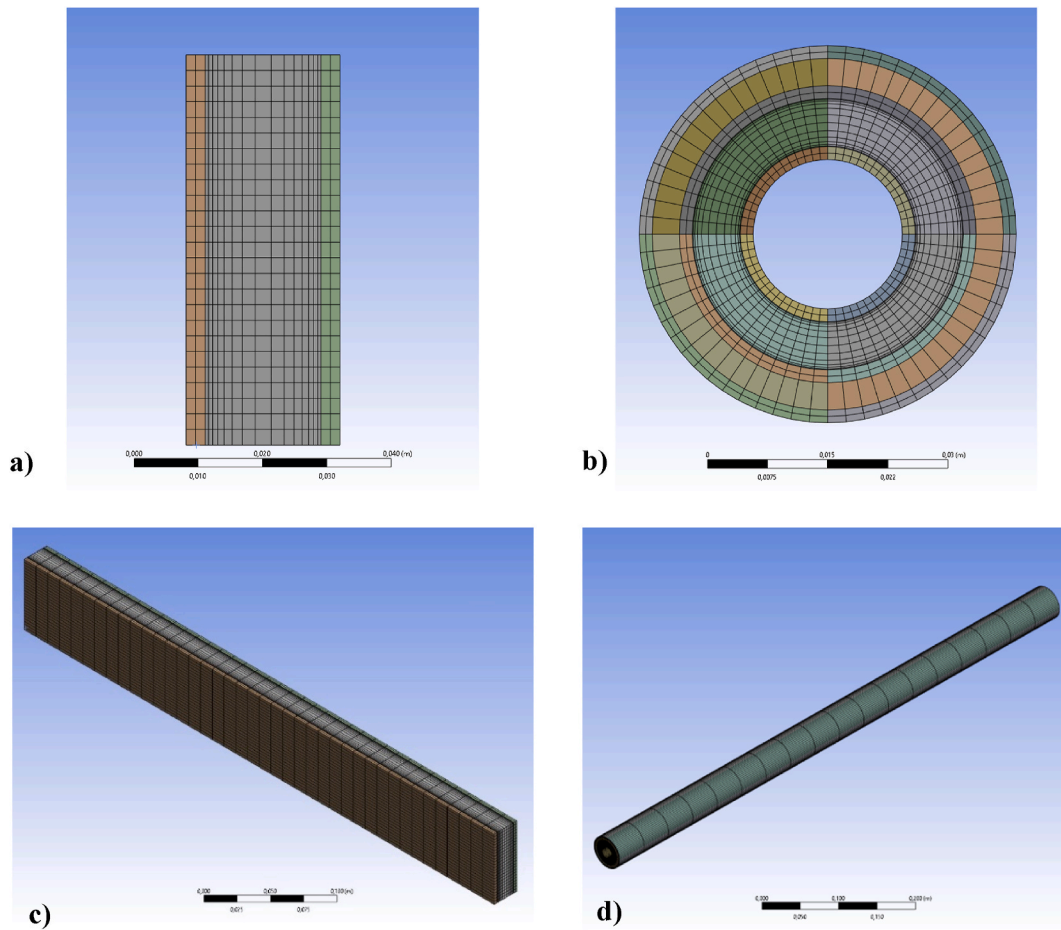| Boundary conditions	Values
T_{amb} [K]	288.15
T_{sky} [K]	296.34
T_{ground} [K]	306.15
h_{ext} [W m^{-2} K^{-1}]	17
ε [−]	0.9 (flat receiver)
	0.9, 0.6, 0.3 (evacuated tube)

Fig. 2. Mesh structure (frontal view and isometric view) for the flat volumetric solar receiver (a-c) and the evacuated tube volumetric solar collector (b-d).
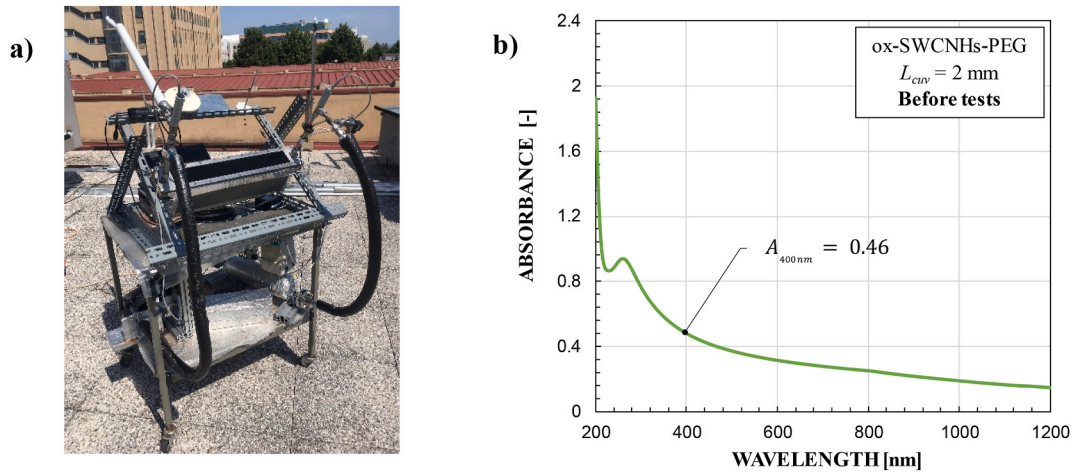

Fig. 3. a) Image of the experimental setup, b) absorption spectrum of the tested nanofluid.

nanofluid temperatures at the inlet and outlet of the receiver, as well as the ambient temperature. Two secondary standard pyranometers are respectively positioned on the front and on the back of the receiver to evaluate the irradiance incident onto the receiver surface G_{inc} and the portion of the solar radiation that is not absorbed by the nanofluid, i.e. the transmitted solar irradiance G_{trans}. The pyranometer on the back of the solar receiver is embedded inside a box which is partially shielded from the solar radiation.

The nanofluid used for the tests consists of a suspension of functionalized SWCNHs (Single-Wall-Carbon-NanoHorns) nanoparticles in deionized water [29]. The nanofluid was prepared using single-wall carbon nanohorns (SWCNHs, provided by Carbonium S.r.l.) at a final concentration of approximately 0.8 g/L.

The SWCNHs were first oxidized using a sulfonitric mixture (H_2SO_4: HNO_3 = 3:1 v/v) in a controlled procedure involving magnetic stirring and three cycles of tip sonication (20 W, 1 min each, 0.3 s ON/0.7 s OFF), followed by further agitation at 45 °C. After centrifugation and purification, the oxidized SWCNHs (ox-SWCNHs) were covalently

functionalized with polyethylene glycol chains (PEG750) through an amidation reaction activated by N-hydroxysuccinimide and EDC·HCl in anhydrous DMF. The reaction mixture was stirred for over 20 h, then purified through precipitation and multiple centrifugation steps to remove unreacted species and solvent residues. The functionalized nanostructures (SWCNH-PEG) exhibited stable dispersion in water without surfactants [30].

The optical stability of the suspension was verified through UV–Vis–NIR absorbance monitoring over a 20-day period. The final suspension, diluted to reach the desired absorbance level, was used to prepare 2 L of nanofluid for use in the experimental test bench. Further details on the synthesis protocol are available in Refs. [24,29].

The absorbance of the nanofluid, shown in Fig. 3b), is measured with a Cary5000 spectrometer using a 0.2 cm quartz cell. The absorbance spectrum of the nanofluid displays a peak at about 265 nm.

In the computational model, the SWCNH-based fluid is treated as a perfectly homogeneous suspension in deionized water. This choice relies on the inherently low van der Waals attractions of SWCNHs, which eliminate the need for surfactants or lengthy sonication to achieve stable dispersions. This assumption is consistent with other numerical studies in the literature and has shown to provide reliable results [15,33,34].

To further support this assumption, the temporal stability of the suspension was experimentally monitored during the thermal efficiency tests used for model validation (total duration: 50 h; flow rate: 5–14 kg h^{-1}; inlet temperature: 27–50 °C). At the end of each test day, small samples were collected and analyzed via UV–Vis–NIR spectroscopy [24]. As shown in Fig. 4, the absorbance at 400 nm decreased from 0.46 to 0.42 over the entire test period, corresponding to a variation of about 9 %. Considering the instrument uncertainty (± 0.01 a.u [35]), this reduction is limited and progressive, with no signs of sedimentation or significant optical degradation. These results confirm that the nanofluid remained substantially stable under the investigated operating conditions, supporting the validity of the homogeneity assumption in the simulation timeframe.

Given the low nanoparticles' concentration and the moderate operating temperatures (up to 50 °C), no significant variation in the thermal properties of the nanofluid was expected or observed during the experimental tests. Measurements performed at the beginning of the experimental campaign confirmed that density and specific heat deviated by less than 1 % compared to pure water, while for dynamic viscosity less than 10 %. Since the thermophysical properties are already very similar to those of the base fluid, minor fluctuations in

nanoparticles' dispersion during the experiments do not lead to appreciable changes in the effective properties and can therefore be considered negligible. Therefore, the nanofluid's properties can be reasonably assumed to remain constant and comparable to those of water throughout the simulation period.

The experimental campaign was performed following the guidelines provided by ISO 9806:2017 Standard [36] to evaluate the absorbed energy fraction (also known as optical efficiency) and the thermal efficiency of the volumetric solar receiver with the varying operating conditions. The absorbed energy fraction of the nanofluid is experimentally obtained using the measurements provided by the two pyranometers:

$$\eta_{opt,exp} = \frac{G_{abs}}{G_{inc} \ \tau_{glass}} = 1 - \frac{G_{trans}}{G_{inc} \ \tau_{glass}^2} \tag{12}$$

where G_{abs} is the absorbed solar irradiance evaluated using Eq. (13), G_{inc} and G_{trans} are respectively the incident and the transmitted solar irradiance measured by the two pyranometers and τ_{glass} is the average transmittance of the glazed area of the receiver (equal to 0.93).

$$G_{abs} = G_{inc} \ \tau_{glass} - \frac{G_{trans}}{\tau_{glass}} \tag{13}$$

More details about the experimental procedure are provided in Ref. [24].

The absorbed energy fraction of the nanofluid can be also calculated analytically starting from the absorbance spectrum of the nanofluid and following the procedure reported in Berto et al. [29]:

$$\eta_{opt,an} = 1 - \tau = 1 - \int f_\lambda \ \tau_\lambda \ \mathrm{d}\lambda \tag{14}$$

In Eq. (14) λ is the wavelength, τ_λ is the spectral transmittance defined as the ratio of the spectral solar irradiance transmitted by the nanofluid $G_{trans,\lambda}$ to the incident spectral solar irradiance $G_{inc,\lambda}$ (Eq. 15), f_λ is the ratio of the spectral incident solar irradiance $G_{inc,\lambda}$ to the total incident irradiance G_{inc} (Eq. 16) and τ is the transmitted energy fraction defined by Eq. (17).

$$\tau_\lambda = \frac{G_{trans,\lambda}}{G_{inc,\lambda}} = \frac{1}{10^{A_\lambda}} \tag{15}$$

$$f_\lambda = \frac{G_{inc,\lambda}}{G_{inc}} \tag{16}$$

$$\tau = \int \tau_\lambda \ \mathrm{d}\lambda \tag{17}$$

In Eq. (15), A_λ is the spectral absorbance of a reference nanofluid, which can be evaluated with a spectrometer using the Lambert Beer law:

$$A_\lambda = L \ \varepsilon_\lambda \ C \tag{18}$$

where L is the path length, ε_λ is the molar extinction coefficient and C is the concentration of nanoparticles in the solution. Considering the values of G_{inc} and $G_{inc,\lambda}$ for the reference Air Mass 1.5 spectral distribution of the solar radiation ([37]) and the values of τ_λ obtained from the absorbance spectrum of the nanofluid, $\eta_{opt,an}$ can be calculated.

From the experiments it is possible to calculate the thermal efficiency of the solar receiver:

$$\eta_{th} = \frac{\dot{m}_n \ c_n \ (T_{out} - T_{in})_n}{G_{inc} \cdot S} \tag{19}$$

where c_n is the nanofluid specific heat, $(T_{out} - T_{in})_n$ is the temperature variation of the nanofluid between inlet and outlet of the solar collector and S is the glazed surface area. The thermal efficiency curve of the receiver is reported against the mean reduced temperature $T_{m,red}$, which is defined as follows:
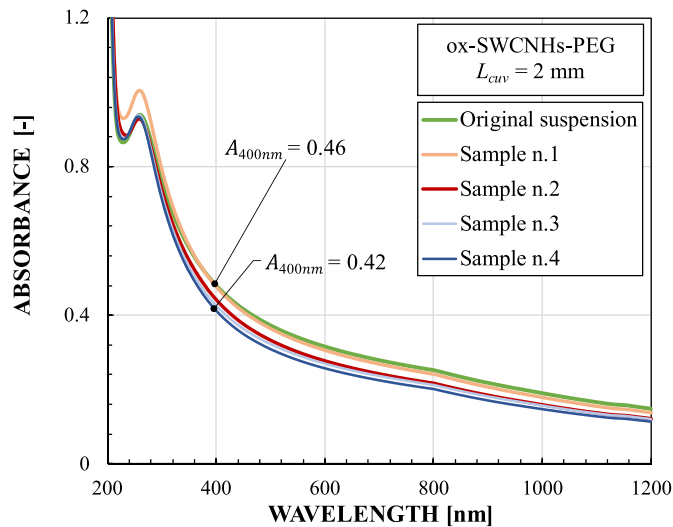

Fig. 4. Absorbance spectra of four carbon nanofluid samples collected during the 50-h experimental campaign used for validation of the numerical model. Measurements were performed with a cuvette path length of 0.2 cm.
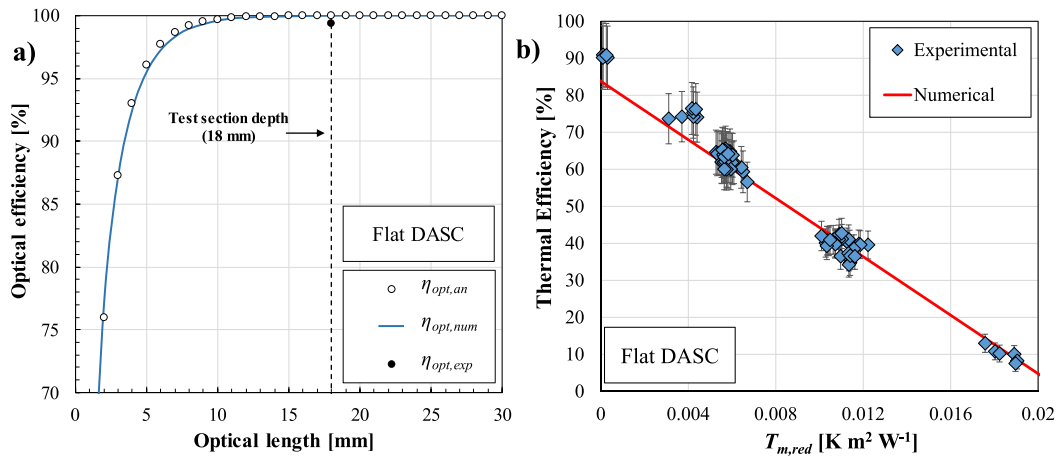
Fig. 5. Validation of the numerical model of the flat DASC in terms of a) optical efficiency and b) thermal efficiency.

$$T_{m,red} = \frac{(T_{out} + T_{in})_n / 2 - T_{amb}}{G_{inc}} \tag{20}$$

The uncertainty related to the measured parameters is evaluated according to the JCGM guidelines [38]. The expanded uncertainty (coverage factor $k = 2$) of the optical efficiency is about 10 %, while for the thermal efficiency it ranges from 4 % to 12 %.

Numerical simulations of the flat DASC are performed with a nanofluid flow rate equal to the experimental one, corresponding to approximately 10 kg h^{-1}. The optical and thermal efficiency of the nanofluid resulting from the simulations are determined by applying Eqs. (12) and (19) to the numerical results. The numerical $\eta_{opt,num}$ and η_{th} values are compared to the experimental ($\eta_{opt,exp}$, evaluated using Eq. 12) and analytical results ($\eta_{opt,an}$, calculated using Eq. 14) in Fig. 5a) and 5b), respectively. A good agreement between the numerical, analytical and experimental optical efficiency values is obtained. The experimental absorbed energy fraction is around 99 % at 18 mm path length, which corresponds to the depth of the flat DASC considered in the present study.

As shown in Fig. 5b), a good agreement can be observed between the experimental thermal efficiency values and those obtained from the simulations, with a mean absolute deviation of 7.5 %. The coefficient of determination R^2 between the experimental data and the numerical results is equal to 0.99. This confirms the accuracy of the numerical model and demonstrates its reliability in assessing the performance of the proposed system.

The slope of the experimental data curve is slightly steeper than the numerical one and this could be due to the simplifications adopted in the modelling of the flat DASC. Indeed, the developed numerical model does not account for the presence of the enclosing box for the back pyranometer and of the surrounding PEEK/steel layers which could be responsible for additional heat exchanges with the environment. Moreover, adiabatic wall boundary condition is set for the inlet, outlet and side walls of the nanofluid, which could lead to a slight underestimation of the occurring thermal losses.

3. Results and discussion

Numerical simulations of both the flat and evacuated tube DASCs under identical operating conditions are conducted to enable a comparative analysis of their performance. The influence of several parameters, including nanoparticles' concentration, nanofluid temperature and mass flow rate, geometrical characteristics and glass properties, on the thermal efficiency of the two DASCs is considered for the comparison.
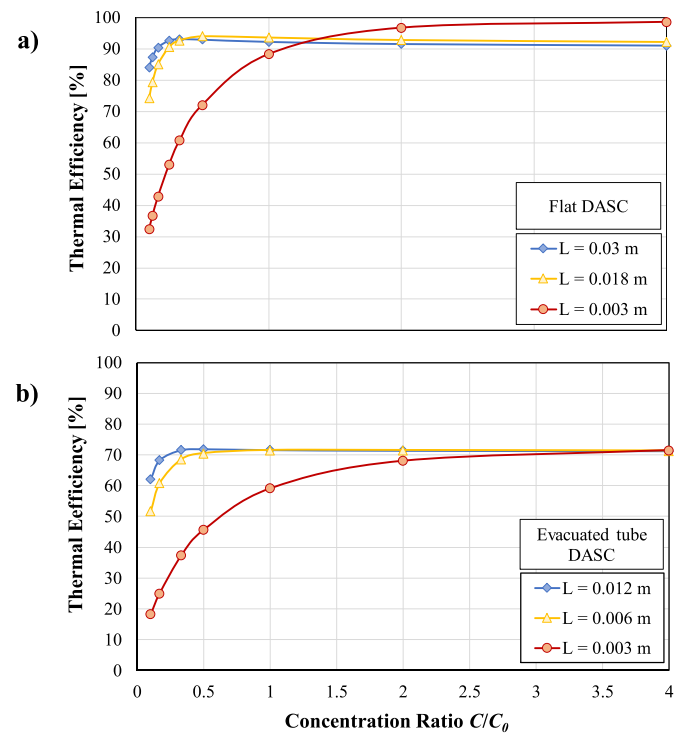

Fig. 6. Trend of thermal efficiency of the flat DASC (a) and the evacuated tube DASC (b), reported versus the ratio of the actual nanoparticles' concentration (C) to the reference one (C_0), at 303.15 K inlet nanofluid temperature (0–0.002 K m^2 W^{-1} mean reduced temperature) and 0.003–0.03 m optical path.

3.1. Effect of nanoparticles' concentration and path length

Numerical simulations are run by varying the nanoparticles' concentration with respect to the one of the tested nanofluid (here indicated with C_0) and the optical path, i.e. by varying the height of the cross-sectional area. In the case of the vacuum-type receiver, the optical length corresponds to the thickness of the annulus where the nanofluid flows and it is modified by varying the diameter of the innermost glass tube. The nanofluid mass flow rate is set to 10 kg h^{-1}, in agreement with ISO 9806:2017 Standard [36].

Fig. 6 shows the comparison between the thermal efficiency of the flat and the evacuated tube DASCs reported as function of the nanoparticles' concentration ratio and the path length, considering an inlet nanofluid temperature of 303.15 K (corresponding to mean reduced

temperatures in the range 0–0.002 K m^2 W^{-1}). As the optical path of the receivers decreases, the maximum efficiency value for the flat DASC shifts towards higher nanoparticles' concentrations (Fig. 6a and b). Indeed, an increase in nanoparticles' concentration results in a shorter optical path required for the absorption of the solar radiation inside the fluid. However, the higher concentration causes an increase of the temperature on the top surface and, therefore, of the heat losses to the environment, which would affect the overall thermal efficiency of the system.

The existence of an optimal nanoparticles' concentration results from the balance between radiation absorption and its ability to propagate through the fluid. At low concentrations, the absorption is weak and much of the incident solar energy passes through the fluid without being effectively converted into heat. At high concentrations, the radiation is mostly absorbed near the fluid surface, causing a non-uniform temperature distribution. The temperatures close to the surface are higher, resulting in increased thermal losses to the environment. This behaviour is supported by the Lambert-Beer law (Eqs. 15 and 18), which relates the attenuation of light to the nanoparticles' concentration and the optical path length. For particles with negligible scattering, such as graphite, the absorption component dominates. An optimal concentration ensures that radiation is absorbed gradually throughout the fluid depth, enabling efficient volumetric heat generation while avoiding excessive surface heating.

In the case of the vacuum-type DASC, increasing the concentration ratio causes the thermal efficiency to rise, up to a maximum value of 71 %, regardless of the optical path length. This plateau can be explained considering that the absorption of the solar radiation is confined to the upper part of the collector, given the direction of the solar rays and the absence of parabolic reflectors in the system modelling. Moreover, the maximum value of thermal efficiency is reached at lower concentration ratios when higher optical path lengths are considered, similarly to the flat DASC.

These considerations are confirmed by Figs. 7 and 8, where the temperature contours at the outlet section for the two DASC geometries are respectively shown for concentration ratios equal to 0.215 and 4.

From the temperature trends, it can be concluded that an increase in nanoparticles' concentration causes solar radiation to be absorbed in the first layers, resulting in a temperature rise and resembling the behaviour of surface collectors. Increasing the nanoparticles' concentration ratio (at a fixed optical path length of 0.018 m) raises the average top-surface temperature of the flat receiver by approximately 2 K (from 306 K at low

concentration to 308 K at high concentration). Although this temperature rise leads to higher convective losses, it also enhances heat transfer to the working fluid, resulting in improved overall efficiency.

At very low concentrations ($C/C_0 = 0.215$), the nanofluid cannot absorb all the incident radiation, so the mean heat flux absorbed by the nanofluid remains stable at around 400 W m^{-2}. As the concentration increases to $C/C_0 = 4$, the absorbed heat flux reaches 450 W m^{-2} and the efficiency rapidly approaches a plateau, since the nanofluid absorbs virtually all the incoming solar energy.

The evacuated receiver exhibits a similar trend, although its circular geometry yields slightly lower efficiencies due to a reduced effective absorption area compared to the flat configuration. It is important to notice that an increase in the nanoparticles' concentration does not necessarily lead to a better thermal performance of the DASCs. Moreover, as shown in Fig. 6, the optimal nanoparticles' concentration is strictly related to the collector geometry. Interestingly, the maximum thermal efficiency for the flat DASC at the selected operating conditions is obtained for a nanoparticles' concentration that is around one third of the tested nanofluid one, if considering the actual optical length (equal to 0.018 m).

In this context, the optical path length, defined as the geometric thickness of the absorbing fluid layer along the direction of incident solar radiation, becomes a key determinant of thermal performance. In direct absorption collectors, where the fluid itself acts as the absorbing medium, the amount and spatial distribution of energy absorption depend not only on the nanoparticles' concentration but also on the depth of the fluid layer that the solar rays traverse.

This concept is particularly relevant when comparing geometries such as flat-plate and evacuated tube collectors. Although evacuated tube DASCs typically contain a larger nanofluid volume, the thermal efficiency under steady-state conditions is primarily influenced by the local optical depth, not by the total fluid volume. For instance, reducing the tube length while maintaining the same optical path does not significantly affect thermal efficiency, since the fundamental radiation–fluid interaction remains unchanged.

Consequently, while the nanofluid volume may influence thermal inertia and dynamic response under transient conditions, steady-state collector performance is dictated more strongly by the interplay between optical properties and geometry to achieve effective volumetric absorption. This underscores the importance of carefully choosing the absorption thickness in accordance with the optical properties of the nanofluid to maximize efficiency and minimize thermal losses.
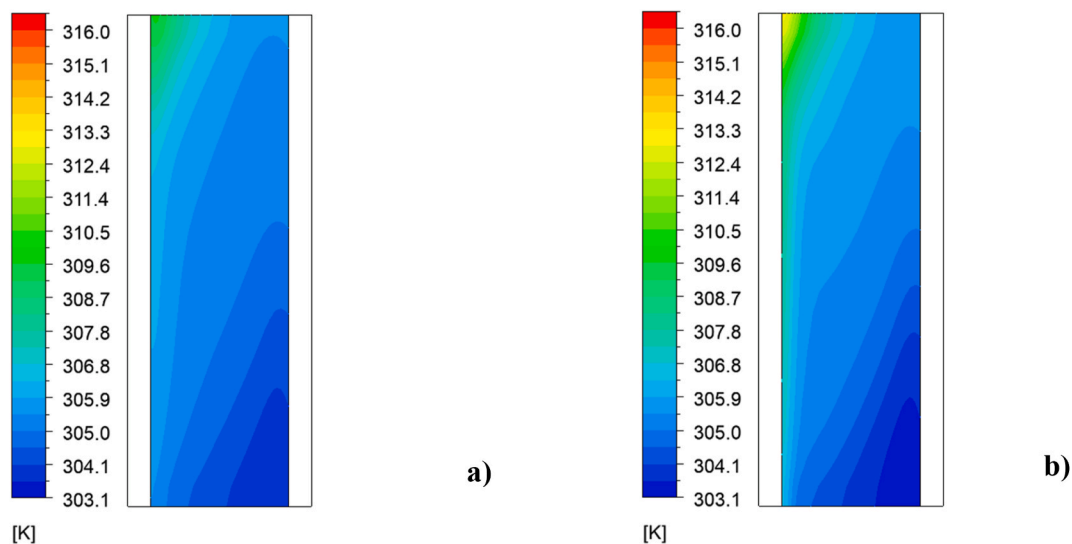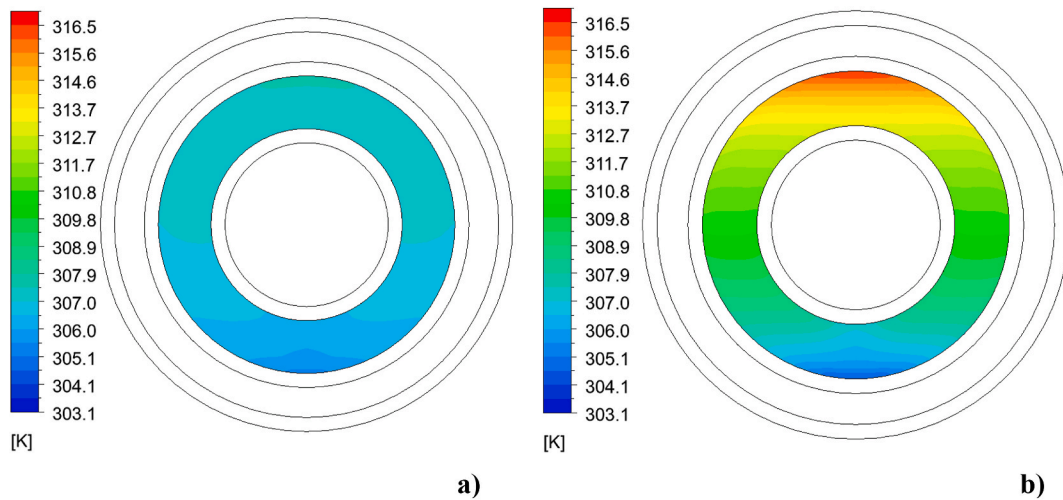

Fig. 7. Temperature contours at the outlet cross section of the flat DASC for concentration ratios of 0.215 (a) and 4 (b), with 303.15 K inlet nanofluid temperature and 0.018 m optical length.

Fig. 8. Temperature contours at the outlet cross section of the vacuum-type DASC for concentration ratios of 0.215 (a) and 4 (b), with 303.15 K inlet nanofluid temperature and 0.006 m optical length.
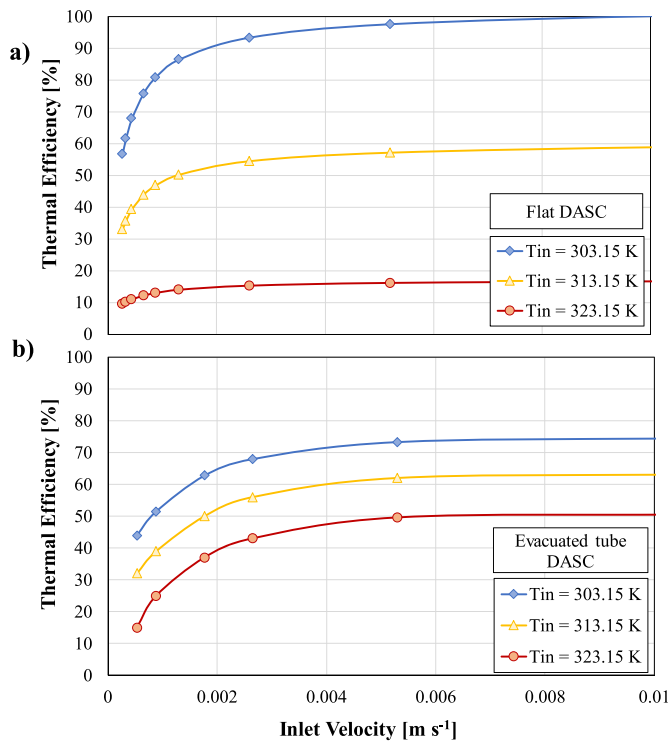
Fig. 9. Trend of thermal efficiency of the flat (a) and the evacuated tube DASCs (b), reported versus the nanofluid inlet velocity at 303.15–323.15 K inlet temperatures (corresponding to mean reduced temperatures between 0 and 0.04 K m^2 W^{-1}), nanoparticles' concentration equal to C_0 and optical length of 0.018 m (a) and 0.006 m (b).

3.2. Effect of nanofluid velocity and temperature

Fig. 9 shows the thermal efficiency of the flat and the evacuated tube DASCs reported as a function of nanofluid velocity and inlet temperature. The nanoparticles' concentration is equal to C_0, while the nanofluid mass flow rate and inlet temperature are respectively varied in the range 1–50 kg h^{-1} and 303.15–323.15 K.

The nanofluid velocity and temperature both influence the thermal efficiency of the flat and the evacuated tube DASCs. As the inlet velocity increases, thermal efficiency rises until it reaches a plateau, because the

temperature distribution inside the receiver becomes more uniform and the thermal losses towards the environment decrease. The dependence of the thermal efficiency on the nanofluid velocity is more marked for the flat DASC since it is more sensitive to temperature variations, via both radiative and convective losses. On the contrary, the vacuum-type DASC is mainly subjected to radiation losses. Moreover, higher thermal efficiency values are reached when the nanofluid inlet temperature in the solar collector is lower, as heat losses to the environment are reduced.

Figs. 10 and 11 respectively show the outlet temperature trends for the flat and the evacuated tube DASCs considering two values of nanofluid velocity, equal to 0.88 mm s^{-1} and 21.2 mm s^{-1}. When the nanofluid velocity at the inlet of the two volumetric receivers is 0.88 mm s^{-1}, higher temperatures are reached at the top volume of the DASC compared to the case at 21.2 mm s^{-1} inlet velocity. This temperature increase leads to higher heat losses to the environment and, consequently, to a thermal efficiency decrease due to sunlight absorption phenomena localized at the surface. Instead, an increase in the nanofluid velocity causes a more uniform temperature distribution inside the DASC, with a consequent improvement of the overall thermal performance of the system.

At very low inlet velocities (0.88 mm s^{-1}), the residence time of the fluid within the system increases, which promotes thermal stratification within the fluid, causing both the surface and outlet nanofluid temperatures to rise. In the flat receiver, the top-surface temperature increases from 306 K at 21.2 mm s^{-1} to 311 K at 0.88 mm s^{-1}, while the outlet temperature rises from 304 K to 308 K over the same velocity range. At the smallest nanofluid velocities, convective losses dominate and overall thermal efficiency decreases. Therefore, the heat flux absorbed by the nanofluid increases from 400 W m^{-2} to nearly 500 W m^{-2}, while convective and radiative losses to the external environment decrease. Above a certain velocity threshold, both temperatures, and hence the thermal efficiency, stabilize at approximately 305 K (close to the surface) and 304 K (close to the outlet section).

### 3.3. Effect of glass properties and collector geometry

To investigate the influence of glass thickness on the thermal performance of volumetric solar receivers, a parametric analysis is carried out by varying the thickness of the glass layers in both flat and evacuated tube receivers. In the flat receiver, the glass thickness is varied from 0.8 mm to 6 mm, while in the evacuated tube receiver it ranges between 0.8 mm and 2.4 mm. All simulations are performed assuming a nanoparticles' concentration ratio equal to 1 and an inlet fluid temperature of
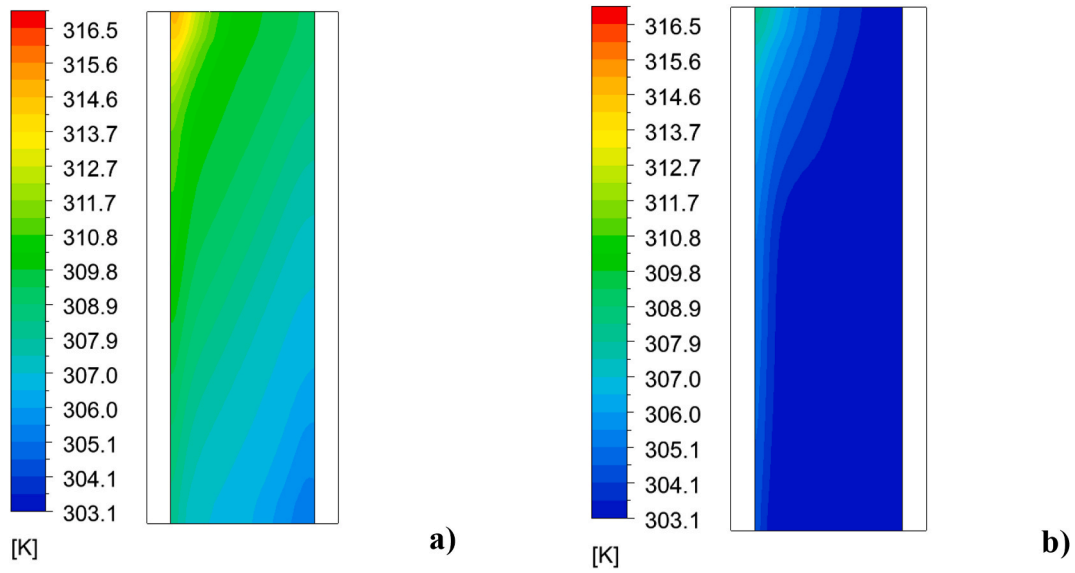
Fig. 10. Temperature contours at the outlet cross section of the flat DASC for inlet velocity of (a) 0.88 mm s^{-1} and (b) 21.2 mm s^{-1} with nanoparticles' concentration equal to C$_0$, 303.15 K inlet temperature and optical length of 0.018 m.
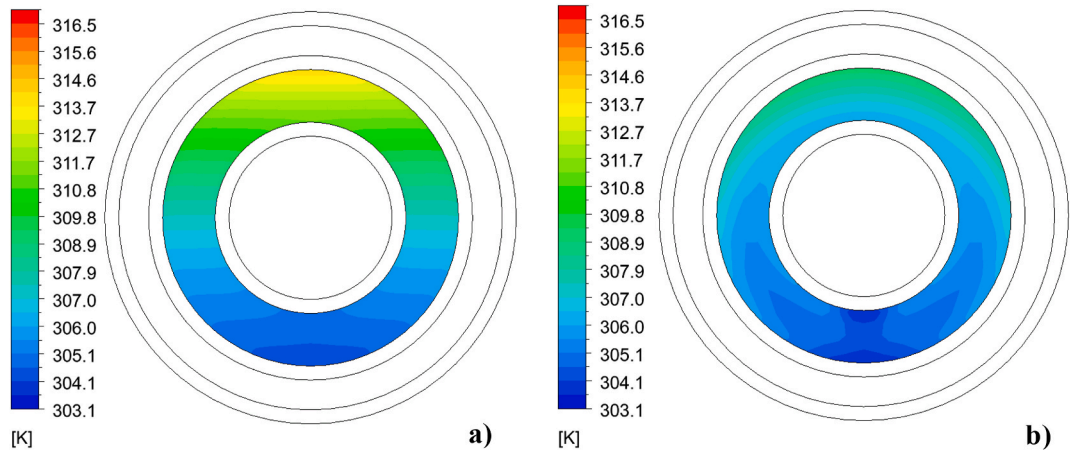
Fig. 11. Temperature contours at the outlet cross section of the evacuated tube DASC for inlet velocity of (a) 0.88 mm s^{-1} and (b) 21.2 mm s^{-1} with nanoparticles' concentration equal to C$_0$, 303.15 K inlet temperature and optical length of 0.006 m.
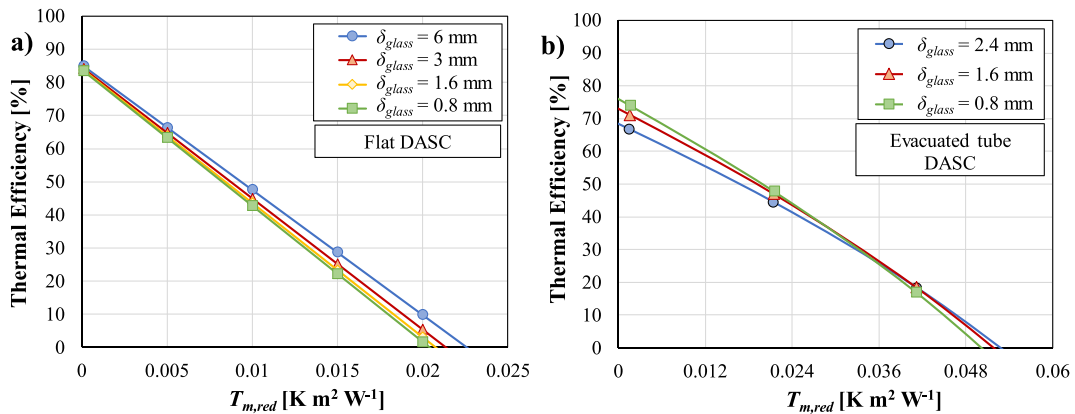
Fig. 12. Effect of glass thickness on the thermal efficiency of flat DASC (a) and evacuated tube DASC (b), reported as function of the mean reduced temperature (nanoparticles' concentration ratio equal to 1, inlet temperature equal to 303.15 K).

303.15 K. The optical path length through the nanofluid is set to 0.018 m for the flat receiver and 0.006 m for the evacuated tube receiver. In the case of the evacuated tube receiver, the outer tube diameter, as well as the nanofluid and vacuum gap thicknesses, are kept constant to isolate the effect of the varying glass thickness. For this reason, glass thicknesses above 2.4 mm are not simulated, as it is not possible to maintain the same configuration beyond this value.

The influence of glass thickness on the thermal performance of both flat-plate and evacuated-tube volumetric receivers is shown in Fig. 12. In the case of the flat receiver, variations in the glass thickness lead only to minor changes in the thermal efficiency at mean reduced temperature $T_{m,r} = 0$ K m^2 W^{-1}, with a mean absolute deviation smaller than 1 % if comparing the 6 mm thick glass case to the 0.8 mm thick glass one. Therefore, when the nanofluid mean temperature is close to the ambient one, the effect of a change in glass transmittance on the thermal efficiency of the collector is negligible. A moderate increase (up to 30 %) in thermal efficiency can be observed at $T_{m,r} = 0.02$ K m^2 W^{-1} mean reduced temperature when the glass thickness is increased from 0.8 mm to 6 mm. This increase is attributed to the additional thermal resistance introduced by the glass layer, which reduces heat losses to the environment.

A similar trend can be observed in the case of the evacuated tube receiver (Fig. 12b). However, in this configuration, increasing the glass thickness results in a deterioration of the optical performance at mean reduced temperature close to zero due to greater reflection losses. At $T_{m,r} = 0$ K m^2 W^{-1} the thermal efficiency decreases by 10 % when the glass thickness is increased from 0.8 mm to 2.4 mm. Indeed, a thicker glass layer increases the probability that incident radiation will be reflected rather than transmitted. Conversely, as the mean reduced temperature increases, the thermal efficiency trend reverses: a thicker glass layer contributes to slightly improved thermal efficiency by reducing heat losses to the environment, similar to what observed for flat collectors.

The effect of applying anti-reflective (AR) coatings to the outer glass of the receiver is also investigated for both collector configurations (Fig. 13). The optical properties of the AR-coated and uncoated glass considered in the simulations are listed in Table 1. These coatings are designed to reduce reflection losses at the air–glass interface by enhancing transmittance, thereby increasing the amount of solar radiation absorbed by the nanofluid.

As a result, a slight improvement in thermal efficiency is observed across the full range of investigated mean reduced temperatures when AR-coated glass is used. This effect is more noticeable in the evacuated tube receiver: with an inlet fluid temperature of 303.15 K, the outlet temperature rises from 309 K (uncoated) to 311 K (AR-coated),
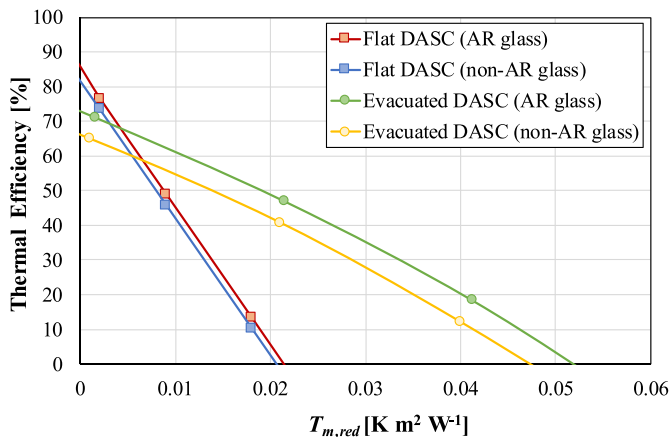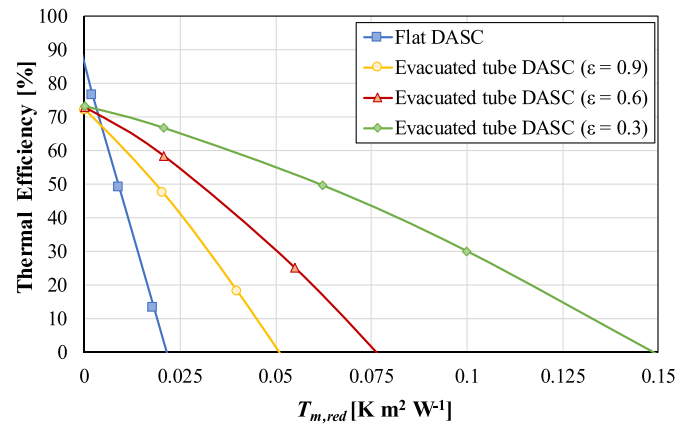

Fig. 14. Thermal efficiency of the flat DASC (emissivity value $\varepsilon = 0.9$) and the vacuum-type receiver (emissivity values $\varepsilon = 0.9$, $\varepsilon = 0.6$ and $\varepsilon = 0.3$) as a function of the mean reduced temperature.

contributing to the observed enhancement in thermal performance.

Fig. 14 reports the thermal efficiency of the two DASCs as a function of the mean reduced temperature. Here, the nanofluid mass flow rate is set to 10 kg h^{-1}, according to ISO 9806:2017 Standard [36]. The nanoparticles' concentration is equal to C_0, while the optical paths are 0.018 m for the flat DASC receiver and 0.006 m for the evacuated DASC receiver.

To account for the different thermal-radiative properties of glazing materials used in solar thermal collectors, emissivity values ε equal to 0.9, 0.6 and 0.3 are selected for the simulations. These values span from untreated clear glass ($\varepsilon = 0.9$) down to advanced low-emissivity coatings ($\varepsilon = 0.3$), in line with values reported in manufacturer datasheets [39] and relevant literature [40–43]. The selected range is representative of commercially available glazing technologies and effectively captures the variation in radiative heat transfer performance relevant to both conventional and volumetric collector configurations.

The evacuated tube DASC displays a smaller thermal efficiency compared to the flat DASC at mean reduced temperature between 0 and 0.005 W m^2 K^{-1}. However, as the mean reduced temperature increases, there is a reversal trend and the evacuated tube receiver becomes more efficient. This behaviour can be explained by considering the difference in terms of thermal losses and optics between the two receivers. Indeed, the evacuated tube DASC displays smaller thermal losses due to the vacuum between the two glass tubes, but also a reduced absorption capability at ambient temperature because its surfaces tend to reflect more. However, Fig. 14 confirms that evacuated tube DASCs could be suitably adopted in a wider range of mean reduced temperatures, without compromising the thermal efficiency of the system. Moreover, the thermal performance of the evacuated tube DASC can be further improved by decreasing the emissivity of the outer glass and, hence, reducing the radiative thermal losses. Indeed, as shown in Fig. 14, at about $T_{m,red} = 0.04$ W m^2 K^{-1} the decrease of the emissivity from 0.9 to 0.6 leads to almost 40 % higher thermal efficiency.

It is important to emphasize that the evacuated tube collector with nanofluid is certainly less efficient compared to a standard evacuated tube collector, especially at high operating temperatures. However, it should be noted that a careful selection of nanoparticles' concentration, which depends on the adopted receiver geometry and particularly on the optical path length, can certainly help improve the performance of direct absorption solar collectors and make them more competitive compared to existing evacuated tube solar collectors.

4. Conclusions

Direct absorption solar collectors (DASCs) represent a promising technology to improve the thermal efficiency of conventional solar

Fig. 13. Effect of glass optical properties on the thermal efficiency of flat DASC and evacuated tube DASCs, reported as function of the mean reduced temperature (nanoparticles' concentration ratio equal to 1, inlet temperature equal to 303.15 K), highlighting the impact of anti-reflective (AR) coating.

thermal devices and decarbonize the building and industrial sectors. In the present study, numerical simulations were conducted in ANSYS Fluent for comparing the thermal performance of a flat direct absorption solar collector and an evacuated tube counterpart, both operating with a Single-Wall-Carbon-NanoHorns (SWCNHs) nanofluid. Such comparative analysis could be helpful to define design guidelines for more efficient and reliable DASCs.

The major outcomes of the present work are the followings:

- The present numerical model was successfully validated in terms of optical and thermal efficiency of the solar receiver using experimental data obtained on a flat DASC,
- From the numerical results, the maximum thermal efficiency of both the DASCs was found at lower nanoparticles' concentration when increasing the optical path length. Such result can be explained considering that the reduction of nanoparticles' concentration would imply a larger optical path for the absorption of the solar radiation inside the fluid. Moreover, the evacuated tube DASC was able to compensate for the major drawback of the considered flat DASC, i.e. its significant loss of thermal efficiency at high operating temperature (320–340 K),
- The temperature profiles inside the receiver depend on the fluid mixing, which is much more intense at high velocities, and on heat losses, which increase as the inlet nanofluid velocity decreases. As a consequence, the thermal efficiency of both DASCs is smaller at low nanofluid velocity, while it reaches a plateau with the increasing velocity, as temperatures are distributed more uniformly inside the collector. A good compromise between nanoparticles' concentration and inlet nanofluid velocity must be achieved to minimize preparation costs and ensure good nanofluid stability,
- With glazing materials having emissivity equal to 0.9, the thermal efficiency of the evacuated tube DASC was about 47 % at mean reduced temperature equal to $0.02 \, \mathrm{W \, m^2 \, K^{-1}}$ while it was almost null in the case of the flat DASC. The thermal performance of the evacuated tube DASC could be further improved by selecting glass tubes with reduced emissivity.
- Increasing the glass thickness reduces thermal losses and enhances thermal efficiency at high mean reduced temperatures, with gains up to 30 % observed for flat receivers. However, it also increases reflection losses, resulting in reduced efficiency at low mean reduced temperatures, with a decrease of about 10 % for evacuated tube configurations. This trade-off is evident for both volumetric collector designs. The application of anti-reflective coatings consistently improves transmittance and thermal performance and is therefore recommended.

To conclude, the design of DASCs must be approached by identifying the optimal nanoparticles' concentration that allows to maximize the thermal efficiency, depending on the geometry of the system, and by minimizing the radiative thermal losses through the use of low-emissivity glasses.

For future implementation of direct absorption solar collector technology, it is important to consider potential cost implications and scalability aspects of the proposed design. The use of Single Wall Carbon Nanohorns (SWCNHs) offers excellent optical properties for the operating fluid, particularly high solar absorption with minimal scattering. However, SWCNHs remain relatively expensive, with market prices between 200 £/g and 750 £/g [44], depending on purity and synthesis method. Despite the low concentrations typically used in nanofluids (0.01–0.1 wt%), the required volumes (several liters) still result in a non-negligible material cost. Economic feasibility will depend on future progress in mass production, dispersion stability and recyclability. However, recent studies have shown that SWCNH-particles can be re-dispersed after sedimentation using sonication or mechanical/-magnetic stirring, supporting their recyclability in long-term applications [24].

In terms of collector layout, the volumetric design introduces simplifications compared to conventional flat plate collectors. Notably, it eliminates the need for a solid absorber plate, which is typically one of the main cost drivers in conventional solar collectors. Such simplification also reduces thermal contact resistances between layers (glass–air–absorber), potentially improving performance and simplifying the overall assembly. Both the volumetric solar receiver geometries considered in the present work are compatible with existing manufacturing technologies, which supports scalability.

For flat plate designs, polymeric housings may reduce costs and conduction losses. The transparent cover, however, plays a more active thermal role and would require low-emissivity glazing, which are typically 2–4 times more expensive than standard glass. In evacuated tubes, the proposed adaptation preserves the existing double-envelope structure, but would require low-emissivity borosilicate coatings, introducing incremental cost but no structural redesign.

In summary, while the proposed volumetric concept adds some cost for advanced materials, it also offers geometrical and functional simplifications, and remains compatible with scalable manufacturing platforms. Further research should address long-term nanofluid stability, cost-effective optical materials and life-cycle cost analysis to support future development.

CRediT authorship contribution statement

Mario Junio Gabellone: Writing – review & editing, Validation, Investigation, Conceptualization, Visualization, Methodology, Data curation, Writing – original draft, Software, Formal analysis. **Arianna Berto:** Validation, Formal analysis, Writing – original draft, Investigation, Conceptualization, Writing – review & editing, Supervision, Data curation. **Emanuele Zanetti:** Writing – review & editing, Conceptualization, Formal analysis, Methodology. **Davide Del Col:** Writing – review & editing, Project administration, Resources, Conceptualization, Supervision, Funding acquisition.

Data availability

Reported data can be made available to the reader upon request to the authors.

Declaration of competing interest

The authors declare the following financial interests/personal relationships which may be considered as potential competing interests:
Davide Del Col reports financial support was provided by European Union - NextGenerationEU, within the Project "Network 4 Energy Sustainable Transition - NEST", Spoke 1, CUP C93C22005230007, Project code PE0000021, funded under the National Recovery and Resilience Plan (NRRP), Mission 4, Component 2, Investment 1.3 - Call for tender No. 1561 of October 11, 2022 of Ministero dell'Università e della Ricerca (MUR). The other authors declare that they have no known competing financial interests or personal relationships that could have appeared to influence the work reported in this paper.

Acknowledgments

Nomenclature

a	Absorption coefficient, m^{-1}
A	Absorbance
c	Specific heat, $\text{J kg}^{-1}\text{ K}^{-1}$
C	Concentration of nanoparticles in the solution, g L^{-1}
E	Total specific energy, $\text{J kg}^{-1}\text{ K}^{-1}$
h_{ext}	Convective heat transfer coefficient, $\text{W m}^{-2}\text{ K}^{-1}$
g	Gravity acceleration, m s^{-2}
G	Irradiance, W m^{-2}
I	Radiation intensity, $\text{W m}^{-2}\text{ sr}^{-1}$
k	Coverage factor
k_{eff}	Effective thermal conductivity, $\text{W m}^{-1}\text{ K}^{-1}$
L	Path length, mm
$\dot{m}$	Mass flow rate, kg h^{-1}
n	Refractive index
p	Pressure, Pa
q	Heat flux, W m^{-2}
S	Glazed surface area, m^2
t	Time, s or h
T	Temperature, K or °C
v	Velocity, m s^{-1}
W	Length, m^{-1}
Greek symbols	
β	Inclination angle, °
ρ	Density, kg m^{-3}
η_{opt}	Optical efficiency
η_{th}	Thermal efficiency
τ	Transmittance
λ	Wavelength, nm
ε_λ	Molar extinction coefficient, $\text{L mm}^{-1}\text{ g}^{-1}$
ε	Emissivity
σ_p	Stefan-Boltzmann constant, $\text{W m}^{-2}\text{ K}^{-4}$
σ_s	Scattering coefficient, m^{-1}
δ	Thickness, m
Subscripts	
λ	Spectral
abs	Absorbed
air	Air
amb	Ambient
an	Analytical
conv	Convective
dew	Dew point
DIF	Diffused
e	Emitted
exp	Experimental
H	Horizontal
glass	Glass layer
ground	Ground facing the DASC
in	Inlet
inc	Incident
m	Mean
n	Nanofluid
num	Numerical
out	Outlet
rad	Radiative
red	Reduced
refl	Reflected
trans	Transmitted
wall	Surface
0	Test conditions (referred to the nanoparticles' concentration)
Abbreviations	
CNT	Carbon NanoTubes
DASC	Direct Absorption Solar Collector
PEG	Polyethylene Glycol
SWCNH	Single Wall Carbon NanoHorn

References

[1] International Energy Agency (IEA), Renewables 2023, Analysis and Forecast to 2028, 2023.

[2] European Commission, UE Directive 2023/2413 amending UE Directive 2018/2001, Renewable Energy Directive (RED III), 2023.

[3] United Nations, Paris Agreement, 2015.

[4] I.E.A. Solar Heating and Cooling Programme, Solar Heat World Wide 2024, 2024.

[5] P.A. Østergaard, N. Duic, Y. Noorollahi, S. Kalogirou, Renewable energy for sustainable development, Renew. Energy 199 (2022) 1145–1152, https://doi.org/10.1016/j.renene.2022.09.065.

[6] P.A. Østergaard, N. Duic, S. Kalogirou, Sustainable development using integrated energy systems and solar, biomass, wind, and wave technology, Renew. Energy 235 (2024) 121359, https://doi.org/10.1016/j.renene.2024.121359.

[7] Z. Said, A.A. Hachicha, S. Aberoumand, B.A.A. Yousef, E.T. Sayed, E. Bellos, Recent advances on nanofluids for low to medium temperature solar collectors: energy, exergy, economic analysis and environmental impact, Prog. Energy Combust. Sci. 84 (2021), https://doi.org/10.1016/j.pecs.2020.100898.

[8] L.A. Omeiza, M. Abid, A. Dhanasekaran, Y. Subramanian, V. Raj, K. Kozak, U. Mamudu, A.K. Azad, Application of solar thermal collectors for energy consumption in public buildings – an updated technical review, J. Eng. Res (2024), https://doi.org/10.1016/j.jer.2023.09.011.

[9] T.B. Gorji, A.A. Ranjbar, A review on optical properties and application of nanofluids in direct absorption solar collectors (DASCs), Renew. Sustain. Energy Rev. 72 (2017) 10–32, https://doi.org/10.1016/j.rser.2017.01.015.

[10] L. Mercatelli, E. Sani, D. Fontani, G. Zaccanti, F. Martelli, P. di Ninni, Scattering and absorption properties of carbon nanohorn-based nanofluids for solar energy applications, J. Eur. Opt. Soc. 6 (2011), https://doi.org/10.2971/jeos.2011.11025.

[11] E. Sani, S. Barison, C. Pagura, L. Mercatelli, P. Sansoni, D. Fontani, D. Jafrancesco, F. Francini, Carbon nanohorns-based nanofluids as direct sunlight absorbers, Opt. Express 18 (2010) 5179, https://doi.org/10.1364/oe.18.005179.

[12] M. Bortolato, S. Dugaria, F. Agresti, S. Barison, L. Fedele, E. Sani, D. Del Col, Investigation of a single wall carbon nanohorn-based nanofluid in a full-scale direct absorption parabolic trough solar collector, Energy Convers. Manag. 150 (2017) 693–703, https://doi.org/10.1016/j.enconman.2017.08.044.

[13] S.M. Henein, A.A. Abdel-Rehim, K. El-Nagar, Energy, economic and environmental analysis of an evacuated tube solar collector using hybrid nanofluid, Appl. Therm. Eng. 219 (2023) 119671, https://doi.org/10.1016/j.applthermaleng.2022.119671.

[14] S. Dugaria, M. Bortolato, D. Del Col, Modelling of a direct absorption solar receiver using carbon based nanofluids under concentrated solar radiation, Renew. Energy 128 (2018) 495–508, https://doi.org/10.1016/j.renene.2017.06.029.

[15] M.H. Yazdi, E. Solomin, A. Fudholi, G. Divandari, K. Sopian, P.L. Chong, Thermal performance of nanofluid flow inside evacuated tube solar collector, Int. J. Heat Technol. 39 (2021) 1262–1270, https://doi.org/10.18280/ijht.390424.

[16] A. Lenert, E.N. Wang, Optimization of nanofluid volumetric receivers for solar thermal energy conversion, Sol. Energy 86 (2012) 253–265, https://doi.org/10.1016/j.solener.2011.09.029.

[17] G. Colangelo, E. Favale, P. Miglietta, A. de Risi, M. Milanese, D. Laforgia, Experimental test of an innovative high concentration nanofluid solar collector, Appl. Energy 154 (2015) 874–881, https://doi.org/10.1016/j.apenergy.2015.05.031.

[18] I.M. Mahbubul, M.M.A. Khan, N.I. Ibrahim, H.M. Ali, F.A. Al-Sulaiman, R. Saidur, Carbon nanotube nanofluid in enhancing the efficiency of evacuated tube solar collector, Renew. Energy 121 (2018) 36–44, https://doi.org/10.1016/j.renene.2018.01.006.

[19] S. Delfani, M. Karami, M.A. Akhavan-Behabadi, Performance characteristics of a residential-type direct absorption solar collector using MWCNT nanofluid, Renew. Energy 87 (2016) 754–764, https://doi.org/10.1016/j.renene.2015.11.004.

[20] P.G. Struchalin, V.S. Yunin, K.V. Kutsenko, O.V. Nikolaev, A.A. Vologzhannikova, M.P. Shevelyova, O.S. Gorbacheva, B.V. Balakin, Performance of a tubular direct absorption solar collector with a carbon-based nanofluid, Int. J. Heat Mass Tran. 179 (2021) 121717, https://doi.org/10.1016/j.ijheatmasstransfer.2021.121717.

[21] A. Moradi, E. Sani, M. Simonetti, F. Francini, E. Chiavazzo, P. Asinari, Carbon-nanohorn based nanofluids for a direct absorption solar collector for civil application, J. Nanosci. Nanotechnol. 15 (2015) 3488–3495, https://doi.org/10.1166/jnn.2015.9837.

[22] S. Wei, L. Espedal, B.V. Balakin, P. Kosinski, Experimental and numerical investigation of direct absorption solar collectors (DASCs) based on carbon black nanofluids, Exp. Heat Transf. (2023) 1–22, https://doi.org/10.1080/08916152.2023.2189327.

[23] M. Simonetti, F. Restagno, E. Sani, M. Noussan, Numerical investigation of direct absorption solar collectors (DASC), based on carbon-nanohorn nanofluids, for low temperature applications, Sol. Energy 195 (2020) 166–175, https://doi.org/10.1016/j.solener.2019.11.044.

[24] A. Berto, N. Mattiuzzo, E. Zanetti, M. Meneghetti, D. Del Col, Measurements of solar energy absorption in a solar collector using carbon nanofluids, Renew. Energy 230 (2024), https://doi.org/10.1016/j.renene.2024.120763.

[25] M. Horie, L.K. Komaba, H. Fukui, H. Kato, S. Endoh, A. Nakamura, A. Miyauchi, J. Maru, E. Miyako, K. Fujita, Y. Hagihara, Y. Yoshida, H. Iwahashi, Evaluation of the biological influence of a stable carbon nanohorn dispersion, Carbon N. Y. 54 (2013) 155–167, https://doi.org/10.1016/j.carbon.2012.11.015.

[26] S. Zhu, W. Niu, H. Li, S. Han, G. Xu, Single-walled carbon nanohorn as new solid-phase extraction adsorbent for determination of 4-nitrophenol in water sample, Talanta 79 (2009) 1441–1445, https://doi.org/10.1016/j.talanta.2009.06.011.

[27] E. Sani, L. Mercatelli, S. Barison, C. Pagura, F. Agresti, L. Colla, P. Sansoni, Potential of carbon nanohorn-based suspensions for solar thermal collectors, Sol. Energy Mater. Sol. Cells 95 (2011) 2994–3000, https://doi.org/10.1016/j.solmat.2011.06.011.

[28] F.R. Menter, Two-equation eddy-viscosity turbulence models for engineering applications, AIAA J. 32 (1994) 1598–1605.

[29] A. Berto, E. Zanetti, G. Ponzana, M. Meneghetti, D. Del Col, In-line measurement of absorbed solar irradiance using a volumetric collector with SWCNH nanofluid, Heat Mass Tran. (2022), https://doi.org/10.1007/s00231-022-03271-6.

[30] E. Zanetti, S. Dugaria, F. Biscaglia, F. Agresti, L. Fedele, M. Meneghetti, D. Del Col, Investigation of nanofluids circulating in a volumetric solar receiver, J. Therm. Sci. Eng. Appl. 13 (2021) 1–12, https://doi.org/10.1115/1.4049041.

[31] L. Mercatelli, E. Sani, A. Giannini, P. Di Ninni, F. Martelli, G. Zaccanti, Carbon nanohorn-based nanofluids: characterization of the spectral scattering albedo, Nanoscale Res. Lett. 7 (2012) 1–5, https://doi.org/10.1186/1556-276X-7-96.

[32] W.H. McAdams, Heat Transmission, third ed., 1954. New York.

[33] M. Akbari, N. Galanis, A. Behzadmehr, Comparative analysis of single and two-phase models for CFD studies of nanofluid heat transfer, Int. J. Therm. Sci. 50 (2011) 1343–1354, https://doi.org/10.1016/j.ijthermalsci.2011.03.008.

[34] A.K. Tiwari, P. Ghosh, J. Sarkar, H. Dahiya, J. Parekh, Numerical investigation of heat transfer and fluid flow in plate heat exchanger using nanofluids, Int. J. Therm. Sci. 85 (2014) 93–103, https://doi.org/10.1016/j.ijthermalsci.2014.06.015.

[35] Agilent, Spectrophotometers Cary 100/300/4000/5000/6000i/7000 User 's Guide, 2021.

[36] ISO, ISO 9806:2017 Standard, Solar Energy - Solar Thermal Collectors - Test Methods, 2017.

[37] ASTM G173-03 Reference spectra (reference air mass 1.5 spectra). https://www.nrel.gov/grid/solar-resource/spectra-am1.5.html (last access: February 17, 2022).

[38] JCGM, Evaluation of Measurement Data - Guide to the Expression of Uncertainty in Measurement, Bureau International des Poids et Mesures (BIPM), Sèvres, France, https://www.bipm.org/en/publications/guides/gum.html (last access: October 29, 2019.

[39] G. Glass, Guardian GlassTime - Technical Manual, 2022.

[40] L. Ma, Z. Lu, J. Zhang, R. Liang, Thermal performance analysis of the glass evacuated tube solar collector with U-tube, Build. Environ. 45 (2010) 1959–1967, https://doi.org/10.1016/j.buildenv.2010.01.015.

[41] F. Giovannetti, S. Föste, N. Ehrmann, G. Rockendorf, High transmittance, low emissivity glass covers for flat plate collectors: applications and performance, Sol. Energy 104 (2014) 52–59, https://doi.org/10.1016/j.solener.2013.10.006.

[42] G. Notton, F. Motte, C. Cristofari, J.L. Canaletti, Performances and numerical optimization of a novel thermal solar collector for residential building, Renew. Sustain. Energy Rev. 33 (2014) 60–73, https://doi.org/10.1016/j.rser.2014.01.061.

[43] B.P. Jelle, S.E. Kalnæs, T. Gao, Low-emissivity materials for building applications: a state-of-the-art review and future research perspectives, Energy Build. 96 (2015) 329–356, https://doi.org/10.1016/j.enbuild.2015.03.024.

[44] INSCX, Global Sales of Nanomaterials, 2021. https://inscx.com/shop/product/titanium-metal-organic-framework-ti-nh2-mil-125-99-30-40μm/ (last access: June 15, 2025).